Author(s): Kawai, Shigeki & Canova, Filippo Federici & Glatzel, Thilo & Foster, Adam S. & Meyer, Ernst

Title: Atomic-scale dissipation processes in dynamic force spectroscopy

Year: 2011

Version: Final published version

Please cite the original version:

Kawai, Shigeki & Canova, Filippo Federici & Glatzel, Thilo & Foster, Adam S. & Meyer, Ernst. 2011. Atomic-scale dissipation processes in dynamic force spectroscopy. Phys. Rev. B. Volume 84, Issue 11. 115415/1-9. ISSN 1550-235X (electronic). DOI: 10.1103/physrevb.84.115415.

Atomic-scale dissipation processes in dynamic force spectroscopy

Shigeki Kawai,[1,*] Filippo Federici Canova,[2,3,†] Thilo Glatzel,[1] Adam S. Foster,[2,3] and Ernst Meyer[1]
[1]*Department of Physics, University of Basel, Klingelbergstrasse 82, CH-4056 Basel, Switzerland*
[2]*Department of Physics, Tampere University of Technology, P.O. Box 692, FI-33010 Tampere, Finland*
[3]*Department of Applied Physics, Aalto University, P.O. Box 11100, FI-00076 Aalto, Finland*
(Received 18 August 2011; published 13 September 2011)

A systematic distance-dependent measurement of the quasistatic tip-sample interactions reveals a hidden stochastic dissipative interaction of the atomic-scale contact in dynamic force microscopy. By comparison of experiment with detailed molecular dynamics simulations, we demonstrate that the infrequently observed hysteresis loops are attributed to the formation of atomic chains during tip retraction. These lead to a large magnitude of energy dissipation in a single cycle and dominate the average measured dissipation, while also leading to differences in the forces measured in static and dynamic force microscopy. This paper provides quantitative force measurements and insights into atomic-scale dissipation processes.

DOI: 10.1103/PhysRevB.84.115415 PACS number(s): 68.37.Ps, 07.79.Lh, 34.20.Cf, 78.66.−w

I. INTRODUCTION

Dynamic force microscopy (DFM) has proven to be an invaluable technique for studying and manipulating nanoscale processes at surfaces.[1–3] In standard imaging, surface topography maps are obtained by keeping a constant frequency shift Δf of a self-oscillating cantilever.[4] The amplitude of this oscillation is maintained by an excitation signal, which provides a direct measurement of the energy dissipated in the system.[5] This dissipative tip-sample interaction in DFM is of importance for investigating, for example, surface mobilities,[6] with the spatial resolution in *damping* often higher than that in topography (see Ref. 7 and references therein). Although the details are far from understood, the high resolution demonstrates that atomic-scale processes induced by the tip-surface interaction dominate dissipation. When the tip apex comes close to the sample surface, deformations of the tip and sample[8] and jumps of atoms between the tip and sample[9,10] lead to a hysteresis loop of the tip-sample interaction force in the approach-retract cycle of a cantilever oscillation.[11,12]

In order to gain detailed insight into the tip-sample interaction forces and the resultant dissipation, it would be very beneficial to make observations over a single oscillation cycle. However, in DFM, the dissipation energy is generally detected via a shift of the excitation ac voltage applied to the piezoactuator to keep a constant oscillation amplitude of the cantilever.[5,13] Due to the narrow measurement bandwidth of the amplitude feedback controller (typically $\approx$100 Hz), the measured energy loss per oscillation cycle is averaged over many cycles ($\gg$100). Although dynamic force spectroscopy (DFS)[14] allows measurements of force and dissipation curves over fixed positions, measurements of individual curves in one oscillation cycle are inherently impossible because of the stochastic nature of the dissipative tip-sample interaction with a finite oscillation amplitude. In contrast, static force spectroscopy (SFS) can directly measure the individual force field upon approach and retraction via the cantilever deflection.[15–17] This technique is widely used for studying adhesion forces on nanometer-scale objects[18] and mechanical properties of biomolecular strings.[19] Contrary to such large systems, dissipative processes on clean and dry surfaces are usually very fast (THz), so that no significant time dependence should exist. As far as we know, a systematic measurement of the atomic-scale interaction with SFS has not been performed.

Here, we report the stochastic tip-sample interaction process by a large number of systematic SFS measurements. We found that infrequently formed atomic chains between the tip and sample give rise to a sudden increase of the dissipation energy in DFM, and the *dynamic force* extracted via the frequency shift differs significantly from the quasistatic force. This is a critical result for quantitative force spectroscopy, and provides a measurement of accurate tip-surface forces. Furthermore, the comparison of experiment and theory provides a detailed description of the atomic processes occurring at contact and insights into their role in energy dissipation.

II. METHODS

A. Experiment

A systematic comparison of SFS and DFS measurements was performed on a clean NaCl(001) surface by our homebuilt ultrahigh vacuum (UHV) atomic force microscope, operating at room temperature.[20] The stiff Si cantilever (Nanosensor NCL-PPP) was annealed in UHV and sequentially sputtered with Ar^+ to clean the tip apex. Before the spectroscopic measurement, the tip was indented into the NaCl surface in order to pick up a NaCl cluster. We performed a SFS measurement at an image maximum (see Fig. 4), where the tip-sample relative position was precisely adjusted with atom-tracked tip positioning before each spectroscopic measurement.

In order to perform systematic distance-dependent measurements of the quasistatic cantilever deflection by SFS and the frequency shift by DFS at room temperature, we designed a complex automated process. This required the management of the scanning parameters in the force microscopy controller by an external computer (Nanonis: SPMCS-PI4). First, the tip-sample relative XYZ position was adjusted by atom-tracked tip positioning[21–23] implemented in DFM with an oscillation amplitude of 1 nm and a frequency shift of -50 Hz. Then, the tip-sample distance feedback was turned off, and the phase and amplitude controllers in the phase-locked loop (PLL) circuit for the cantilever self-oscillation were sequentially switched off. Subsequently, the ac excitation voltage to the

dither piezoactuator for the cantilever excitation was set to 0 V. After the amplitude decreases to the level of the thermal oscillation amplitude, the sample surface was approached toward the tip apex by an oscillation amplitude of 1 nm. Since the cantilever is mounted with a tilt angle of ≈13° in our system, the sample was also moved by 230 pm in the Y direction. Then, the distance dependence of the quasistatic cantilever deflection Δz_{def}, with a z sweep distance of 2 nm and a certain different initial z distance z_{ini}, was measured.[24] The sample was retracted by 1.5 nm, and the amplitude and phase controllers in the PLL circuit as well as the tip-sample z feedback were sequentially turned on. z_{ini} was changed from 2.27 to 1.67 nm with a step of 30 pm (21 curves).

These 21 approach-retract sweeps with different z_{ini} were repeated 100 times. Each SFS measurement took ≈13 s and the total measurement took 792 min. In order to perform reliable switches between dynamic and static modes, the small oscillation amplitude used in atom-tracked tip positioning is mandatory due to a small but critical error of the amplitude calibration. Therefore, the second flexural mode of a silicon cantilever was used in order to realize the small amplitude DFS measurement with high effective stiffness.[25,26] Moreover, the high resonance frequency of ≈1 MHz shortens the duration of the amplitude drop after switching off the ac excitation voltage to the dither piezoactuator.[27] The effective spring constant $k_{2\mathrm{nd}}$ of the second mode (1624 N/m) was calibrated by bimodal DFS with equal amplitudes of the first and second flexural modes ($A_{1\mathrm{st}} = A_{2\mathrm{nd}} = 10$ nm).[28] The static stiffness of the cantilever k_0 was calibrated via the first resonance frequency. k_0 of 27.7 N/m was high enough to prevent cantilever jump-into-contact instabilities.

The vertical force was calculated as $F = -k_0 \Delta z_{\mathrm{def}}$ and the relative cantilever support-sample distance z_s was rescaled to the relative tip apex-sample distance by $z_c = z_s - \Delta z_{\mathrm{def}}$. The origin of the tip-sample z distance is defined at a distance which was adjusted by atom-tracked tip positioning with a frequency shift $\Delta f_{2\mathrm{nd}}$ of −50 Hz and $A_{2\mathrm{nd}}$ of 1 nm.

B. Theory

1. Simulation details

Simulations are carried out using our molecular dynamics software, CUstiC (CUDA Atomistic Code),[29,30] that integrates the equation of motion for a system of ions using the Leapfrog algorithm with a time step of 1 fs. The analytical expressions for interatomic forces can be found by deriving the total energy with respect to atomic coordinates, and are implemented in our code so that the evaluation is performed on the graphics processing unit (GPU). This is the most expensive operation and is performed on the GPU in order to take advantage of its massively parallel architecture, which gives more than 100-fold speedup compared to a normal CPU implementation of the same algorithm.

The total potential energy of the system can be written as

$$U = \sum_{i \neq j} k \frac{q_i q_j}{r_{ij}} + \sum_{i \neq j} \left(A_{ij} e^{-\frac{r_{ij}}{\rho_{ij}}} + \frac{B_{ij}}{r_{ij}^6} \right), \qquad (1)$$

where q_i are the ion charges, r_{ij} is the distance between ionic pairs and A_{ij}, B_{ij}, and ρ_{ij} are parameters defined for each kind of ionic pair. The first term is the long-range electrostatic interaction, and the second represents the short-range Buckingham-type interaction.[31] The parameters for all ionic pairs were obtained from previous studies[32–34] and are listed in Tables I and II.

TABLE I. Mass and charge parameters for the ions present in the simulated system.

Ion	Mass (a.u.)	Charge (a.u.)
Na	23.0	1.0
Cl	35.4	−1.0
Mg	24.3	2.0
O	16.0	−2.0

The software is specifically designed to simulate a system consisting of a surface and an atomic force microscopy (AFM) tip, and to mimic the motion of the tip in a real AFM experiment. In this particular case the tip was forced to oscillate harmonically above the surface as in a DFM/DFS experiment: The oscillation amplitude was set to match the experimental value of 1 nm, but the frequency was increased to 100 MHz in order to reduce the simulation time and make it affordable. We believe this choice does not have a big impact on the results since, even though the simulated tip moves 100 times faster than the real one, it is still four orders of magnitude slower than the vibrational frequencies of the system (THz regime) that determine the details of the atomic motion. To check this assumption we performed several simulations with oscillation frequencies ranging from 100 GHz to 100 MHz, but we could not see any significant difference in the results obtained below 500 MHz. All our simulations are carried out with the thermostats set at 300 K.

While the simulation runs, the tip is gradually displaced vertically, following the harmonic oscillation, and the forces acting on the atoms in the tip are recorded at every step, averaged out over 1000 steps (i.e., 1 ps) and printed in the output. This way we can obtain the force curves for the approach and retract phases, and the dissipated energy during the cycle E_d can be obtained as

$$E_d = \oint \vec{F}\, d\vec{s}, \qquad (2)$$

TABLE II. Buckingham-type interaction parameters for the ionic pairs in our system.

Pair	A (eV)	ρ (Å)	B (eVÅ^6)
Na-Na	6927.80	0.1863	−4.430
Na-Cl	3046.40	0.2836	−12.82
Cl-Cl	2021.30	0.3588	−88.98
O-Na	1677.83	0.2934	−0.000
O-Cl	4393.10	0.2721	−62.20
O-O	9574.96	0.2192	−32.00
Mg-Na	28261.4	0.1510	−2.100
Mg-Cl	2511.51	0.2857	−6.220
Mg-O	1284.38	0.2997	−0.000
Mg-Mg	0.00	1.0	0.0

where $\vec{F}$ is the total force on the tip and the integration runs through the oscillation cycle. This is effectively calculated using the trapezoidal integration rule. The choice of printing the average value of the total force every 1000 steps allows us to see fast changes in the tip. It should be noted that the total force on the tip contains only contributions from the atoms in the system, but long-range, *background*, van der Waals interactions between the macroscopic tip and the sample are excluded. The tip has a virtual point (called *marker*) attached to it that moves with the tip holder during the harmonic oscillation, and is used to define the tip-sample distance; all our tips (see the next section for details) have the marker in the average position of the apex atom calculated after relaxing the tip in vacuum. The tip-sample distance calculated in this way is then shifted by a constant offset in order to obtain the best agreement between the simulated dissipation and experimental data. The optimal offset was found to be 0.45 nm.

The software initializes several copies of the system with different random initial velocities drawn from the Maxwell-Boltzmann distribution and then performs the simulation for every copy at the same time. This is the same as repeating the simulation to gather better statistics, but we do it simultaneously to exploit the full potential of the GPU. Only the lower half of the cycle is simulated in order to further reduce the simulation time.

2. *Model system*

The simulated system consists of a NaCl slab of size $10 \times 10 \times 4$ atoms (Fig. 1); since there are no periodic boundary conditions, the lower atomic layer and all atoms on the edge of the slab were frozen. The one next to the last atomic layer and all the atoms adjacent to the frozen edges are strongly coupled to a Berendsen thermostat. All the other atoms are treated as Newtonian, with no thermostat directly applied. This way the thermostat does not introduce any artificial feature in the region of interest where the tip interacts with the surface and it prevents any possible collective oscillation from being reflected by the frozen edge.

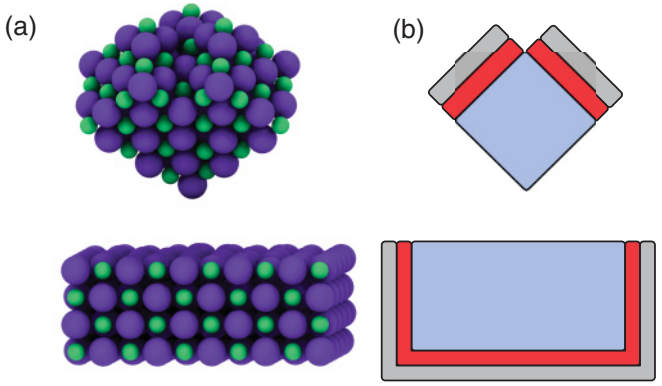

FIG. 1. (Color online) (a) Snapshot of a model surface and tip. The surface and the tip are made of Na (green/gray) and Cl (purple/dark gray) atoms. (b) Schematic two-dimensional (2D) view of the system: The blue (medium gray) area represent free Newtonian atoms, the red (dark gray) parts consists of atoms coupled to the thermostat, and the grayed area stands for the frozen boundary.

The choice of the tip is more critical and we had to test several options before being able to reproduce the experimental behavior. The base topology for the tip consists of a $4 \times 4 \times 4$ atoms cube: Since the real tip is indented in the NaCl surface, it is reasonable to start with a crystalline NaCl cube rotated in order to expose one corner to the surface. The three faces pointing upward are extended with one atomic layer coupled to the thermostat, and one more atomic layer of fixed atoms:[35] These extensions can be regarded as the *tip holder* since they do not interact strongly with the surface and are necessary to preserve the symmetry of the model tip (Fig. 1). This ideal tip gives a very small hysteresis, leading to 5 meV/cycle at most, as it is very stable and no evident tip change was seen. We tested a series of tips built using this one as a starting point, introducing vacancies and impurities, and although in some cases we could calculate higher dissipation, these tips often led to surface decoration; the average energy dissipation was always smaller than the experimental one.

Finally, we started building the tip following a procedure similar to the experiment itself. We start from an ideal MgO tip [Fig. 2(a)], with the same shape as the one in Fig. 1. The four bottom layers are cut and several atoms were removed at random in the middle of the resulting cluster: this models a rough, polar, oxidized tip. The tip is made to oscillate close to a NaCl slab $10 \times 10 \times 6$ atoms wide, so that it will be pushed deep into the slab to simulate the indentation process [Fig. 2(b)] happening at the beginning of the experiment. After retraction,

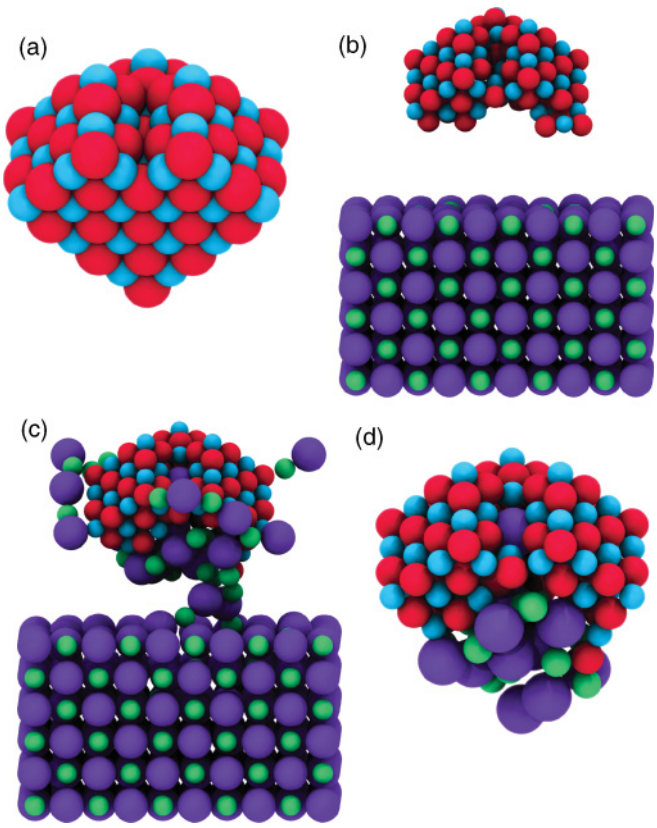

FIG. 2. (Color online) (a) Ideal MgO tip. (b) Rough MgO tip with a larger NaCl slab. (c) Resulting tip after indentation. (d) Final cleaned tip. O are red (gray), Mg are cyan (light gray), Na are green (medium gray), and Cl atoms are purple (dark gray).

the MgO holder picked up a NaCl nanocluster from the surface [Fig. 2(c)]: A few atoms that jumped to the upper part of the tip are removed manually afterward, since that volume would be occupied by the oxide material in the rest of the tip. The final tip is separated from the surface [Fig. 2(d)] and relaxed in vacuum for 1 ns. Due to the mismatch in the MgO and NaCl lattice constants the NaCl nanocluster is in a disordered phase.

III. RESULTS

A. Experiment

1. Distance dependence of the quasistatic cantilever deflection

Figure 3 shows several examples of quasistatic vertical interaction force curves in approach-retract cycles measured via the cantilever deflection signal Δz_{def} at six different z_{ini}. While the closest tip-sample z distance ($=z_{\mathrm{ini}} - 2\ \mathrm{nm} - \Delta z_{\mathrm{def}}$) in one approach-retract cycle becomes smaller, the magnitude of the tip-sample attractive force increases, and a hysteresis loop appears. The large attractive tip-sample interaction gives rise to deformations of the tip apex and/or sample. It is worth noting that an instability of the tip apex is more likely to happen than a cantilever jump-into-contact event.

Figure 4(a) shows a series of example quasistatic vertical interaction approach and retraction force curves measured via SFS for different z_{ini}. Across the 100 measurements at each z_{ini}, we observed that the force measured is highly stochastic, with significant variation in the approach and retraction curves. The area of the hysteresis loop in one SFS approach-retraction cycle corresponds to a certain energy loss or dissipation (E_{d}).[17] Most often, the approach and retraction force curves have a similar character and the measured dissipation clusters around zero. However, every so often there are *spikes* in the dissipation where an order of magnitude increase in energy dissipated per cycle is seen—these spikes are relatively rare, but dominate

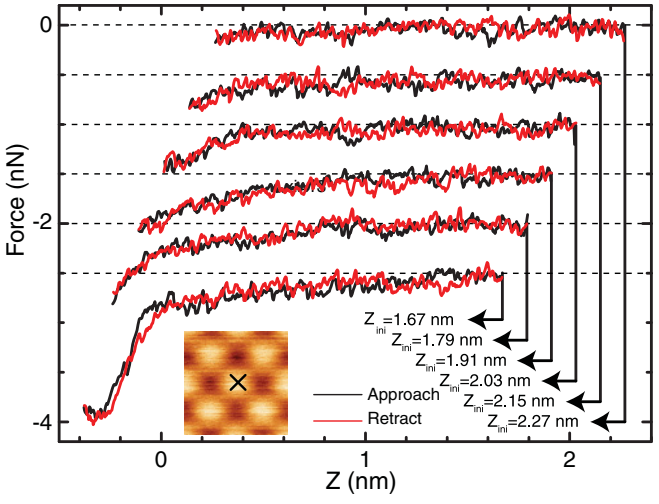

FIG. 3. (Color online) Distance dependence of quasistatic vertical interaction force in approach and retract, measured in SFS with different initial z position z_{ini} on the maxima observed in DFM. The inset image was obtained with $A_{2\mathrm{nd}} = 1.0$ nm at $\Delta f_{2\mathrm{nd}} = -40$ Hz. The vertical axes of each curve are shifted by 0.5 nN. Measurement parameters: $k_0 = 27.7$ N/m.

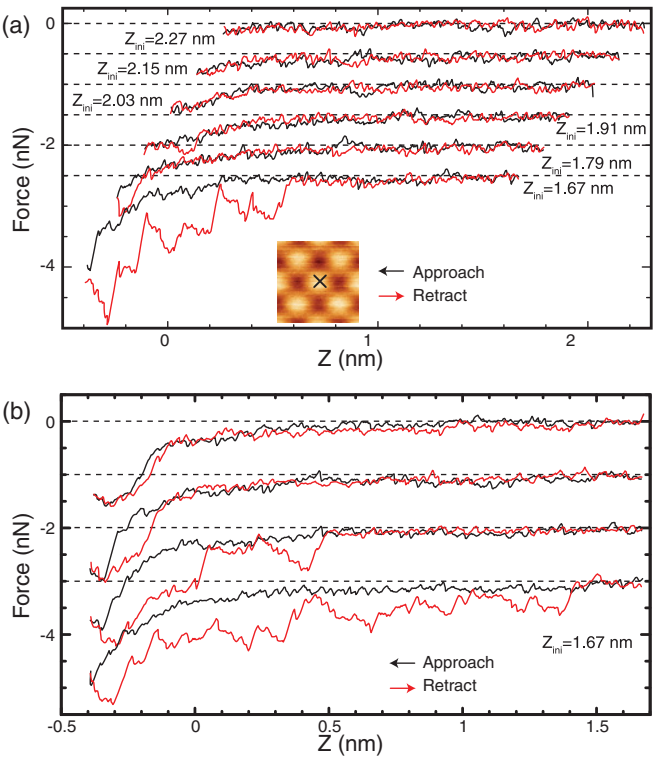

FIG. 4. (Color online) (a) SFS force curves for a 2-nm approach and retraction measured with a variety of different initial z positions (z_{ini}) over maxima in DFM images [see the inset image, obtained with $A_{2\mathrm{nd}} = 1.0$ nm at Δf of the second flexural mode ($\Delta f_{2\mathrm{nd}}$) = -40 Hz]. Each curve is shifted by 1 nN with respect to the previous for clarity. (b) A set of example force curves from measurements with closest approach, i.e., smallest z_{ini}.

the average dissipation per cycle ($\bar{E}_{\mathrm{d}}$). The magnitude of these spikes and their frequency increases as the tip approaches closer to the surface. In order to show the character of the hysteresis, Fig. 4(b) shows a series of approach and retraction curves from $z_{\mathrm{ini}} = 1.67$ nm. This is an extreme example at closest approach, but it demonstrates the character of the differences in approach and retraction that are responsible for the measured dissipation.

2. Distinct frequency shift

If one sweep in the SFS measurement is regarded as one oscillation cycle of the cantilever, the corresponding frequency shift Δf can be calculated via the measured approach-retract force curve as

$$\Delta f = -\frac{f}{2\pi k A}\int_0^{2\pi} \bar{F}(z_0 + A\cos\theta)\cos\theta\, d\theta, \qquad (3)$$

where f is the resonance frequency, k the stiffness, A the amplitude, $\bar{F}$ the tip-sample quasistatic force averaged over approach and retract, and z_0 the equilibrium tip-sample distance.[36] The parameters for the calculation were taken from those of DFS ($f = 975\,673$ Hz, $k = 1624$ N/m, $A = 1$ nm). Figure 5 summarizes the histograms of the calculated Δf for the different z_{ini}. Assuming that the atomic processes causing the tip change are much faster than both one SFS sweep ($\approx$13 s) and a DFM oscillation cycle (1 μs), they are effectively

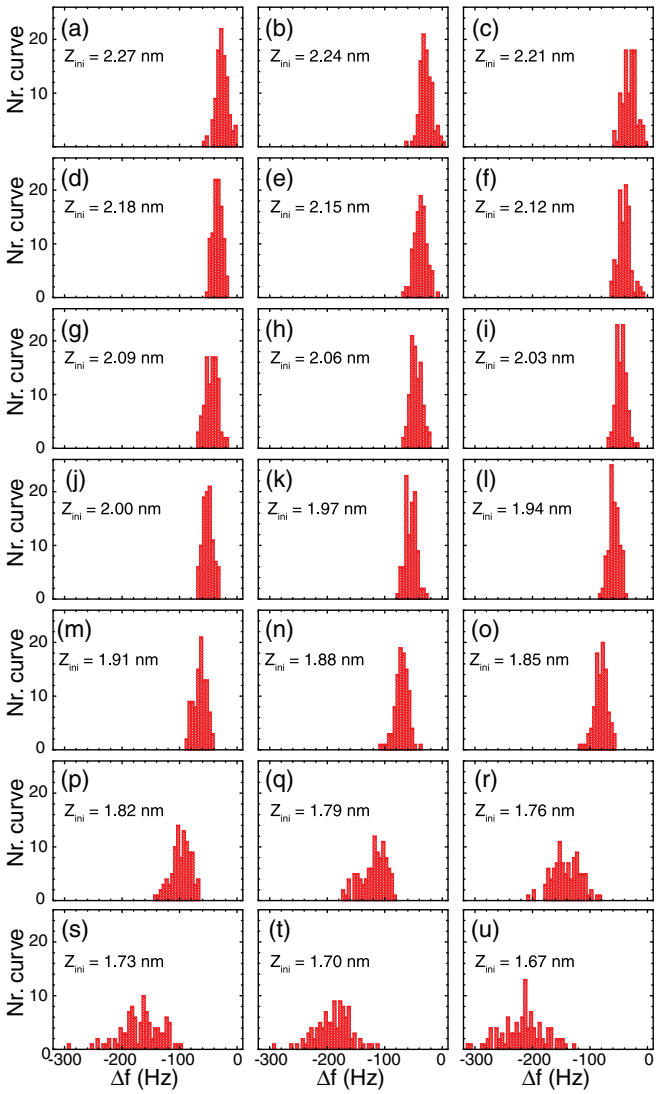

FIG. 5. (Color online) Histogram of the calculated frequency shift Δf via the quasistatic force curves measured by SFS on NaCl(001) with a sweep distance of 2 nm and 21 different initial z positions. Calculation parameters: $f = 975\,673$ Hz, $k = 1624$ N/m, and $A = 1$ nm.

time independent at the experimental scale and the histograms in Fig. 5 correspond to the Δf spectrum of the oscillating cantilever in DFM.

The Δf averaged over 100 curves corresponds to the measured Δf at z_0 ($=z_{\rm ini} - A - \bar{\Delta z}_{\rm def}/2$), where $\bar{\Delta z}_{\rm def}$ is the time-averaged cantilever deflection over one sweep and can be calculated as[24]

$$\bar{\Delta z}_{\rm def} = \frac{1}{2\pi k_0}\int_0^{2\pi} \bar{F}(z_0 + A\cos\theta)d\theta. \qquad (4)$$

Since the fluctuation of the stochastic tip-sample interaction force in one cantilever sweep modulates the magnitude of the time-averaged cantilever deflection, the determination of averaged z_0 in the SFS measurement is not a trivial issue. Moreover, the tip-sample interaction force is detected via the cantilever deflection—the closest tip-sample distance in one sweep is not constant. Hence z_0 is further modulated by the stochastic tip-sample interaction. Therefore, the Δf calculated via the quasistatic force is, strictly speaking, influenced by the increased tip-sample attractive force at the turning point closer to the sample surface by $\Delta z_{\rm def}$. Since in the measurement the Z scanner controls the cantilever support-sample distance, and not directly the tip-sample distance, and $\Delta z_{\rm def}$ is changed by the stochastic tip-sample interaction, we have to take care in the definition of closest approach in this discussion. Specifically, $\Delta z_{\rm def}$ for calculations of Δf via the $\bar{F}$ force upon approach and retraction in Fig. 12 was taken as an average from 100 curves. The difference due to the definition of the closest approached tip-sample distance appears when significant dissipative interaction is present.

3. *Distinct dissipation energy*

The area of the hysteresis loop of one approach-retraction cycle corresponds to the energy dissipated in that cycle, and can be calculated as

$$E_{\rm d} = \int_{z_0-A}^{z_0+A} [F_{\rm app}(z) - F_{\rm ret}(z)]dz, \qquad (5)$$

where $F_{\rm app}$ and $F_{\rm ret}$ are the approach and retraction force curves, respectively.

Figure 6 summarizes the histograms of the $E_{\rm d}$ calculated from SFS force curves, for the different $z_{\rm ini}$. Contrary to the histograms of Δf (Fig. 5), the standard deviation of $E_{\rm d}$ is large even at large tip-sample separation. This is due to the process of the numerical treatment, and the calculation of $E_{\rm d}$ suffers from low-frequency noise due to the subtraction between $F_{\rm app}$ and $F_{\rm ret}$, while the calculation of Δf smoothens out the noise by the integration. Some loops with high-energy dissipation were detected at close approach ($z_{\rm ini} < 1.76$ nm) and are highlighted in the plots by the green (light gray) area. The unusually large hysteresis area in these loops is caused by major tip changes.

Figure 7 shows the mean energy dissipation $\bar{E}_{\rm d}$ calculated from the histograms, including and excluding the curves with highly dissipative loops. Although the number of the curves with big tip change features is small, the overall $\bar{E}_{\rm d}$ increases by a factor of 2 at the smallest tip-sample separation.

B. Simulations

We simulated several consecutive DFS loops using the tip obtained through indentation, and we repeated the simulation with different approach distances: in all cases, at least 20 consecutive loops were performed, although a few simulations were continued longer to investigate tip degradation.

Figure 8 summarizes the energy dissipation calculated at an approach distance of $z = 0$ nm; while the simulations at other approach distances were performed only for 20 consecutive cycles, this one in particular was let go until 43 cycles were computed. It can be seen from the trend of the average energy dissipation that our tip tends to become more stable as the simulation time passes. While some of the first ten cycles form a chain, almost none do so after 30 cycles. From the snapshot of the tip in Fig. 8 we can see how the initially disordered NaCl nanocluster at the end of the tip is now reconstructed in a crystalline lattice, quite similar to the one of the ideal NaCl tip in Fig. 1. This happens because after approach, an atomic

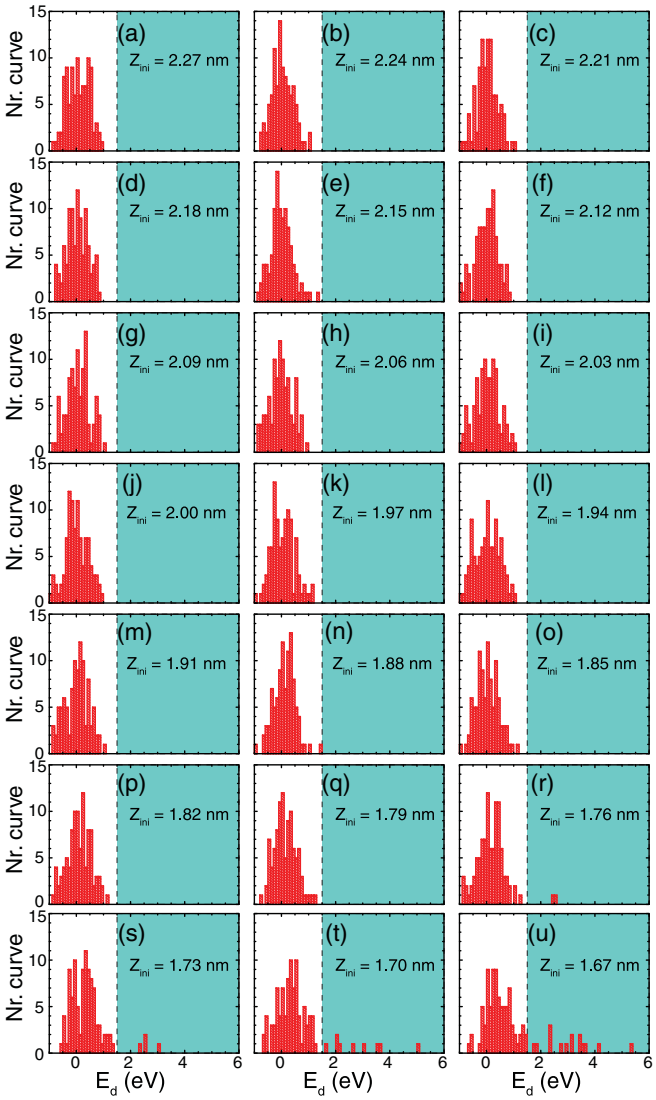

FIG. 6. (Color online) Histogram of the energy dissipation E_d calculated from the quasistatic force measured by SFS on NaCl(001).

chain can diffuse from the tip, and the few atoms pulled out are already a considerable amount of material for the small NaCl nanocluster. When the chain breaks, most of the apex atoms are in an undercoordinated state, and the whole nanocluster can access a more stable state. A larger tip, with a bigger NaCl nanocluster, would be able to give longer chains, and have many more metastable states so that the crystalline phase would be less accessible regardless of the number of cycles.

Figure 9 shows histograms of the energy dissipation calculated at different approach distances (0.1, 0.15, and 0.2 nm) in the first 20 loops; at higher distances there are less cycles with high-energy dissipation, less chains are formed, and the average dissipation is lower (see Fig. 11). As the tip oscillates closer to the surface, more chains can be pulled from the tip, thus increasing the overall dissipation, in agreement with the experiment. When the tip-sample distance is further reduced, we calculate force curves exhibiting the typical behavior of indentation measurements and the dissipation increases even more.

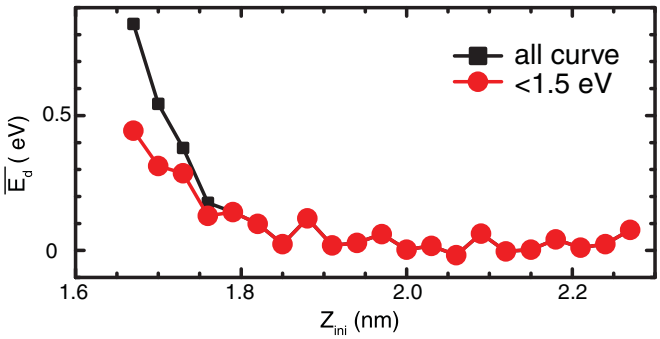

FIG. 7. (Color online) Mean energy dissipation $\bar{E}_d$ via the histogram at each tip-sample separation, including and excluding the curves with highly dissipative loops.

Figure 10 shows the results of such a simulation. The NaCl nanocluster in the tip apex is pushed against the surface so that more atoms are effectively interacting with the surface; as the tip retracts, the adhesion causes a large hysteresis area between −0.25 and 0.05 nm, giving a dissipation of 0.556 eV: After this point a chain is formed, dissipating another 0.71 eV. While this adhesive process is present in all the simulated cycles (it is less intense after tip degradation), the chain formation process is still stochastic, although it is more likely to occur in this range of distances due to the strong tip-surface interaction.

The series of force curves is plotted in Fig. 11, along with the calculated $\bar{E}_d$ for the whole cycle: The fact that we see several different shapes reflects the stochastic nature of the process seen in the SFS experiment and also reproduces the wide hysteresis loops seen in experiments. The atomic trajectories from the simulations show that these highly dissipative events are due to the formation of atomic chains (Fig. 11 inset) and that longer chains are responsible for higher dissipation, e.g., see the last two force curves in Fig. 11. The shape of the hysteresis loops is similar in character to that observed during soft indentation into metal surfaces and the associated formation of atomic chains.[37,38] A similar

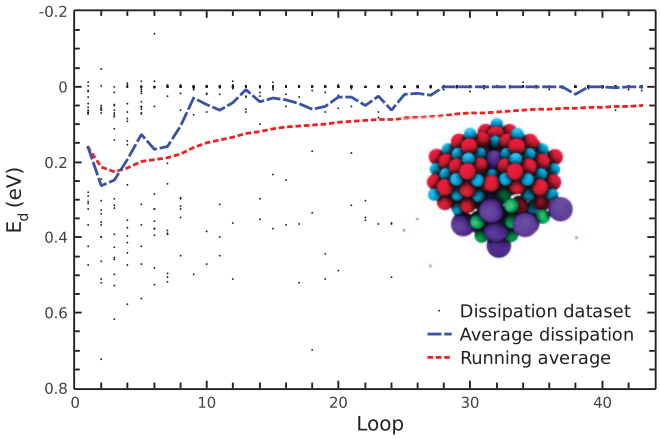

FIG. 8. (Color online) (Dots) Dissipation dataset calculated from each loop. (Blue/dashed line) Dissipation averaged at each loop between the 20 replicae of the experiment. (Red/short dashed line) Overall dissipation running average. The tip approach distance is $z = 0$ nm. The inset shows a snapshot of the tip after 40 cycles.

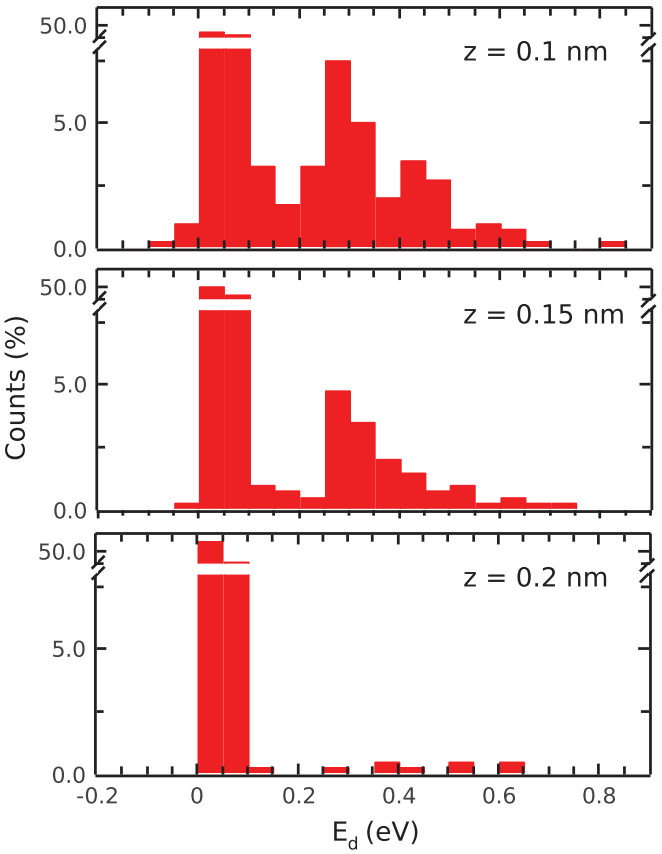

FIG. 9. (Color online) Histograms of the calculated energy dissipation at different approach distances: 0.1, 0.15, and 0.2 nm. The vertical axes are cut to show the higher dissipative loops.

phenomenon, although with a different mechanism, has been suggested theoretically for ionic materials.[39]

When the whole dataset of recorded cycles is considered, although there are loops dissipating up to 0.7 eV when the longest chain is formed, these are effectively a small subset in

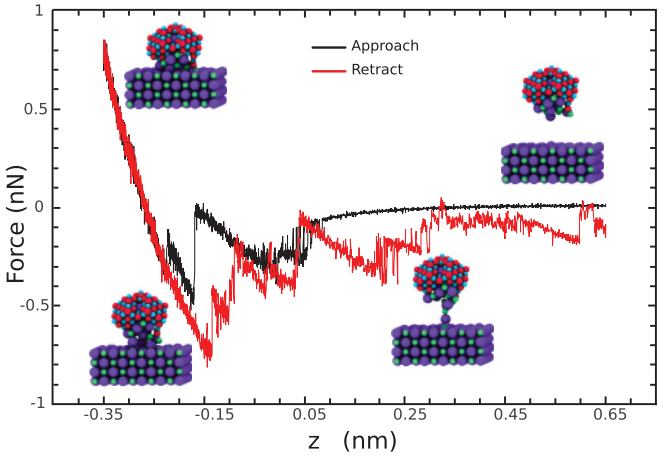

FIG. 10. (Color online) Typical force curve calculated with a maximum approach distance of 0.1 nm: Approach and retract curves are represented by black and red (gray) lines, respectively. A few snapshots of the system were put along the force curve to show the indentation process.

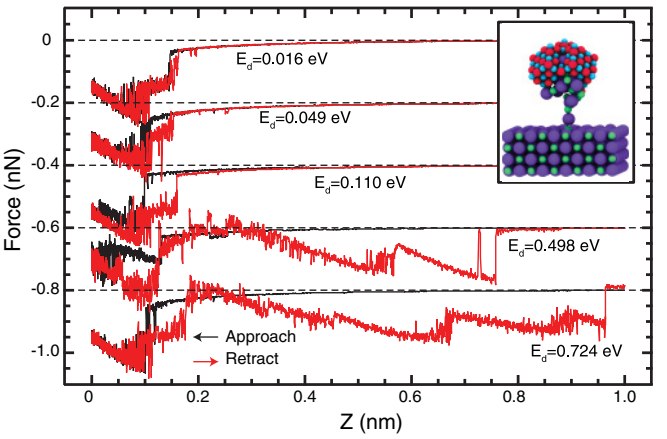

FIG. 11. (Color online) A series of approach and retraction force curves selected from our simulations with increasing dissipation. Each curve was shifted by 0.2 nN. The inset shows a snapshot from the simulations.

the many simulated loops, while most loops present smaller chains (one or two atoms long) or no chain at all, thus the average dissipation is lower. Formation of long, highly dissipative chains is a rare event, as in the experimental results. The simulations also point out that the chain is made entirely from the Na and Cl atoms in the tip's nanocluster, and, in

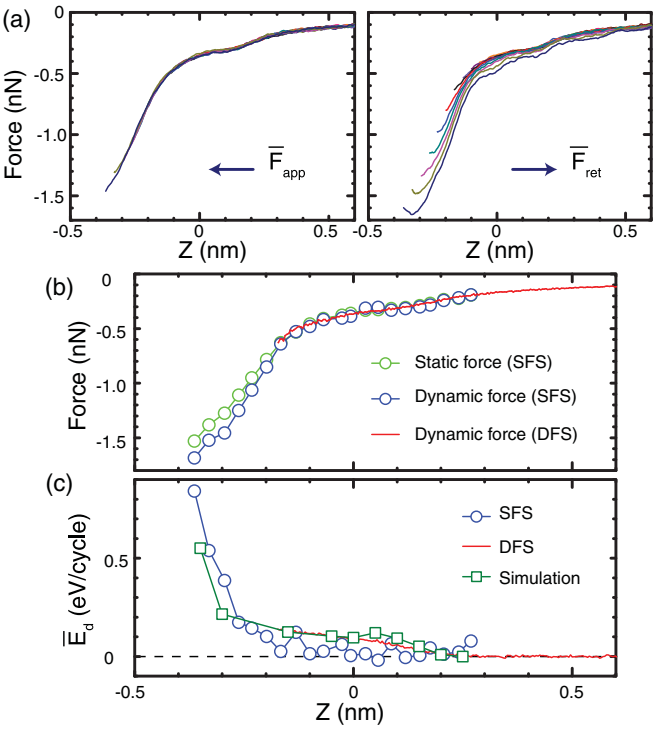

FIG. 12. (Color online) (a) Average force for 21 different z_{ini}, averaged over 100 SFS measurements upon approach ($\bar{F}_{app}$) and retraction ($\bar{F}_{ret}$). (b) Total average force. Here the static force is directly taken from the SFS measurements, while the dynamic force (SFS) is a virtual DFS measurement based on the SFS data. The dynamic force (DFS) shows the measured DFS average force. (c) Comparison of average dissipation ($\bar{E}_d$) as a function of z from SFS and DFS measurements, and MD simulations at the same atomic site.

agreement with experimental observations, when the chain breaks, every atom returns to the tip (in 99.97% of cases), leaving the surface clean.

IV. DISCUSSIONS

Figure 12(a) shows the average of each set of 100 SFS curves for every z_{ini} upon approach ($\bar{F}_{\mathrm{app}}$) and retraction ($\bar{F}_{\mathrm{ret}}$). Note that all the approach curves are very similar, indicating that the dissipative process occurs after closest approach and there are no significant tip changes that survive a full approach-retraction cycle. Combined with the stability of the atom tracking during the measurement and the lack of surface modification seen in atomically resolved DFM images, this implies that the dissipative processes occur during the initial stages of retraction and mainly involve atoms in the tip. Note that although the hysteresis in approach and retraction forces was pointed out theoretically as an origin of dissipated energy,[11,12,40] this time the curves have been extracted experimentally—the stochastic nature of the hysteresis loop means that the average curves given by DFS hide many of the details of the individual cycles provided by SFS.

Figure 12(b) shows a comparison of the total average force measured in SFS and DFS. Here we see the inherent limitation in DFM—at very close approach we see the onset of instabilities and a high probability of a tip crash. In order to compare the SFS and DFS measurements over the full distance range, we combined the measured $\Delta f_{2\mathrm{nd}}$ from DFS with the predicted $\Delta f_{2\mathrm{nd}}$ for the measured SFS forces to give a *virtual* dynamic force curve from the SFS data.[41] At relatively large tip-sample separations, where average dissipation is small, the three distance-dependent curves have similar characteristics. However, at small tip-sample separations, the extracted dynamic force varies significantly from the measured static force. This phenomenon shows that the dynamic force is affected by the dissipative tip-sample interaction and this may be important at much larger tip-surface distances in more dissipative systems.

In Fig. 12(c), the measured $\bar{E}_{\mathrm{d}}$ in SFS and DFS is compared. As discussed earlier, in SFS $\bar{E}_{\mathrm{d}}$ is calculated from the hysteresis of the approach and retraction force curves. In DFS, the average energy loss per one oscillation cycle is obtained as $\bar{E}_{\mathrm{d}} \approx E_0(A_{\mathrm{exc}} - A_{\mathrm{exc},0})/A_{\mathrm{exc},0}$, where E_0 is the intrinsic loss of energy per oscillation cycle in the cantilever, and A_{exc} and $A_{\mathrm{exc},0}$ are the damped and undamped excitation amplitudes respectively.[5] The magnitude of $\bar{E}_{\mathrm{d}}$ measured in DFS was significantly larger than that in SFS in the z range of the DFS measurement. Since E_{d}, measured with the same tip at the same atomic site with a smaller $A_{2\mathrm{nd}}$ of 0.5 nm, shows a comparable characteristic curve, the reason for the inconsistency is not related to electrostatic interactions.

Repeating the simulation with different approach distances, we obtained the distance dependence of $\bar{E}_{\mathrm{d}}$, plotted in Fig. 12(c), in quantitative agreement with both experimental results. Both SFS measurements and simulations approach significantly closer to the surface than the DFS measurements, and both give a rapid increase in dissipation. The simulations show that the tip is now indenting the surface, and the resulting large displacements of surface atoms combined with increased chance of chain formation produce higher dissipation—the large instabilities at such a close approach make conventional DFS impossible. The formation of chains also gives a likely explanation for the differences in $\bar{E}_{\mathrm{d}}$ measured in DFS and SFS. For DFS, an individual point at a certain z distance is recorded in 12 ms and the cantilever (frequency of 1 MHz) oscillates for 12 000 cycles. The simulations are an average over 400 cycles, while the SFS is averaged over 100 sweeps. The comparison of SFS, DFS, and simulations clearly shows how increased statistics gives better sampling and raises $\bar{E}_{\mathrm{d}}$ as more dissipation spikes are included.

Out of the several tips we tested, this was the only NaCl-based tip that could show the same dissipation processes seen in the SFS experiment. More idealistic NaCl tip models give little dissipation and oxide-based models caused irreversible tip changes. Note that the differences in absolute magnitude of calculated and measured dissipation in a single cycle are due to differences between the model tip and experimental reality. First, we know very little about the atomic structure of the tip, save that it is NaCl based and the model can only represent a best guess. Second, the computational expense scales dramatically with the system size, and we are restricted to relatively small tip sizes if we wish to obtain good statistics—this limits our capability to model the extensive atomic processes at a very close approach and the resulting long chains. Effectively this means that chains form more often in the simulations, but are shorter on average—the longest length of the chain estimated from measurements was $\approx$1.8 nm [estimated from Fig. 4(b)], whereas the maximum in simulations was $\approx$1.0 nm. Nevertheless, the qualitative agreement in the hysteresis in forces and the quantitative agreement in $\bar{E}_{\mathrm{d}}$ shows that the simulations capture the key atomic processes.

V. CONCLUSIONS

We investigated the atomic-scale interaction by a systematic static force spectroscopic measurement. The extracted "dynamic force" differs from the "quasistatic force" due to the stochastic dissipative tip-sample interaction. In general, this provides a standard for accurate tip-surface interaction measurements, particularly in systems where significant dissipation can be expected.[23,42] Furthermore, the agreement between experiments and simulations demonstrates that atomic chain formation is a rare but key process that produces a dissipation *spike* and dominates the average energy dissipation. This is a key step toward a complete understanding of atomic-scale dissipation at contact. Important next steps are to examine how tip functionalization could be used to further control dissipated energy and to study other surfaces where we would expect differences in chain formation probability[3]—preliminary studies on the Cu(111) surface show similar features, but with a significant increase in chain length.

ACKNOWLEDGMENTS

This work was supported in part by the Swiss National Science Foundation and NCCR "Nanoscale Science," the ESF FANAS programme, and the Finnish Academy of Science and Letters. The authors thank Alexis Baratoff for valuable discussions.

*shigeki.kawai@unibas.ch
†filippo.federici@tut.fi

[1] S. Morita, F. J. Giessibl, and R. Wiesendanger, *Noncontact Atomic Force Microscopy*, Vol. 2 (Springer, Berlin, 2009).
[2] O. Custance, R. Perez, and S. Morita, Nat. Nanotechnol. **4**, 803 (2009).
[3] C. Barth, A. S. Foster, C. R. Henry, and A. L. Shluger, Adv. Mater. **23**, 477 (2011).
[4] F. J. Giessibl, Rev. Mod. Phys. **75**, 949 (2003).
[5] B. Anczykowski, B. Gotsmann, H. Fuchs, J. P. Cleveland, and V. B. Elings, Appl. Surf. Sci. **140**, 376 (1999).
[6] M. Ashino, D. Obergfell, M. Haluka, S. Yang, A. N. Khlobystov, S. Roth, and R. Wiesendanger, Nat. Nanotechnol. **3**, 337 (2008).
[7] F. F. Canova and A. S. Foster, Nanotechnology **22**, 045702 (2011).
[8] A. Schirmeisen, D. Weiner, and H. Fuchs, Phys. Rev. Lett. **97**, 136101 (2006).
[9] R. Hoffmann, A. Baratoff, H. J. Hug, H. R. Hidber, H. V. Löhneysen, and H.-J. Güntherodt, Nanotechnology **18**, 395503 (2007).
[10] S. A. Ghasemi, S. Goedecker, A. Baratoff, T. Lenosky, E. Meyer, and H. J. Hug, Phys. Rev. Lett. **100**, 236106 (2008).
[11] N. Sasaki and M. Tsukada, Jpn. J. Appl. Phys. **39**, L1334 (2000).
[12] L. N. Kantorovich and T. Trevethan, Phys. Rev. Lett. **93**, 236102 (2004).
[13] T. R. Albrecht, P. Grütter, D. Horne, and D. Rugar, J. Appl. Phys. **69**, 668 (1991).
[14] M. A. Lantz, H. J. Hug, R. Hoffmann, P. J. A. van Schendel, P. Kappenberger, S. Martin, A. Baratoff, and H. J. Güntherodt, Science **291**, 2580 (2001).
[15] S. P. Jarvis, H. Yamada, S.-I. Yamamoto, H. Tokumoto, and J. B. Pethica, Nature (London) **387**, 247 (1996).
[16] G. Cross, A. Schirmeisen, A. Stalder, P. Grütter, M. Tschudy, and U. Dürig, Phys. Rev. Lett. **80**, 4685 (1998).
[17] G. L. W. Cross, A. Schirmeisen, P. Grütter, and U. T. Dürig, Nat. Mater. **5**, 370 (2006).
[18] E. L. Florin, V. T. Moy, and H. E. Gaub, Science **264**, 5157 (1994).
[19] J. P. Junker, F. Ziegler, and M. Rief, Science **323**, 633 (2009).
[20] L. Howald, E. Meyer, R. Lüthi, H. Haefke, R. Overney, H. Rudin, and H. J. Güntherodt, Appl. Phys. Lett. **63**, 117 (1993).
[21] D. W. Pohl and R. Möller, Rev. Sci. Instrum. **59**, 840 (1988).
[22] M. Abe, Y. Sugimoto, O. Custance, and S. Morita, Appl. Phys. Lett. **87**, 173503 (2005).
[23] S. Kawai, T. Glatzel, S. Koch, A. Baratoff, and E. Meyer, Phys. Rev. B **83**, 035421 (2011).
[24] S. Kawai, T. Glatzel, S. Koch, B. Such, A. Baratoff, and E. Meyer, Phys. Rev. B **80**, 085422 (2009).
[25] S. Kawai, S. Kitamura, D. Kobayashi, S. Meguro, and H. Kawakatsu, Appl. Phys. Lett. **86**, 193107 (2005).
[26] S. Kawai, F. Rose, T. Ishii, and H. Kawakatsu, J. Appl. Phys. **99**, 104312 (2006).
[27] S. Kawai and H. Kawakatsu, Appl. Phys. Lett. **89**, 013108 (2006).
[28] S. Kawai, T. Glatzel, S. Koch, B. Such, A. Baratoff, and E. Meyer, Phys. Rev. Lett. **103**, 220801 (2009).
[29] J. E. Stone, D. J. Hardy, I. S. Ufimtsev, and K. Schulten, J. Mol. Graphics Modell. **29**, 116 (2010).
[30] L. Nyland, M. Harris, and J. Prins, *GPU Gems 3*, Vol. 31 (Addison-Wesley, Boston, MA, 2007), Chap. 31, pp. 677–695.
[31] R. A. Buckingham, Proc. R. Soc. London A **168**, 264 (1938).
[32] M. J. L. Sangster and R. M. Atwood, J. Phys. C **11**, 1541 (1978).
[33] R. W. Grimes, C. R. A. Catlow, and A. M. Stoneham, J. Phys. Condens. Matter **1**, 7367 (1989).
[34] A. L. Shluger, A. L. Rohl, D. H. Gay, and R. T. Williams, J. Phys. Condens. Matter **6**, 1825 (1994).
[35] A. I. Livshits and A. L. Shluger, Phys. Rev. B **56**, 12482 (1997).
[36] F. J. Giessibl, Phys. Rev. B **56**, 16010 (1997).
[37] U. Landman, W. D. Luedtke, N. A. Burnham, and R. J. Colton, Science **248**, 454 (1990).
[38] G. Rubio-Bollinger, S. R. Bahn, N. Agraït, K. W. Jacobsen, and S. Vieira, Phys. Rev. Lett. **87**, 026101 (2001).
[39] A. L. Shluger, L. N. Kantorovich, A. I. Livshits, and M. J. Gillan, Phys. Rev. B **56**, 15332 (1997).
[40] J. E. Sader, T. Uchihashi, M. J. Higgins, A. Farrell, Y. Nakayama, and S. P. Jarvis, Nanotechnology **16**, S94 (2005).
[41] J. E. Sader and S. P. Jarvis, Appl. Phys. Lett. **84**, 1801 (2004).
[42] B. J. Albers, T. C. Schwendemann, M. Z. Baykara, N. Pilet, M. Liebmann, E. I. Altman, and U. D. Schwarz, Nat. Nanotechnol. **4**, 307 (2009).